

Please cite the Published Version

Slate, AJ, Hickey, NA, Butler, JA, Wilson, D, Liauw, CM, Banks, CE and Whitehead, KA (2021) Additive manufactured graphene-based electrodes exhibit beneficial performances in *Pseudomonas aeruginosa* microbial fuel cells. *Journal of Power Sources*, 499. ISSN 0378-7753

DOI: <https://doi.org/10.1016/j.jpowsour.2021.229938>

Publisher: Elsevier

Version: Accepted Version

Downloaded from: <https://e-space.mmu.ac.uk/628068/>

Usage rights:  [Creative Commons: Attribution-Noncommercial-No Derivative Works 4.0](https://creativecommons.org/licenses/by-nc-nd/4.0/)

Additional Information: Author accepted manuscript published by and copyright Elsevier.

Enquiries:

If you have questions about this document, contact openresearch@mmu.ac.uk. Please include the URL of the record in e-space. If you believe that your, or a third party's rights have been compromised through this document please see our Take Down policy (available from <https://www.mmu.ac.uk/library/using-the-library/policies-and-guidelines>)

Additive Manufactured Graphene-based electrodes exhibit beneficial performances in *Pseudomonas aeruginosa* microbial fuel cells

Anthony J. Slate^{1,2,3,*}, Niall A. Hickey², Jonathan A. Butler⁴, Daniel Wilson⁴,
Christopher M. Liauw², Craig E. Banks^{3,4} and Kathryn A. Whitehead^{2*}

¹: *Department of Biology and Biochemistry, University of Bath, Claverton Down, Bath, BA2 7AY, UK.*

²: *Microbiology at Interfaces, Faculty of Science and Engineering, Manchester Metropolitan University, Chester Street, Manchester M1 5GD, UK*

³: *Manchester Fuel Cell Innovation Centre, Manchester Metropolitan University, Chester Street, Manchester M1 5GD, UK*

⁴: *Faculty of Science and Engineering, Manchester Metropolitan University, Chester Street, Manchester M1 5GD, UK*

⁴: *Department of Mechanical Aviation and Civil Engineering, Faculty of Science and Engineering, University of Manchester, Sackville Street Building, Manchester M1 3WE, UK*

*To whom correspondence should be addressed.

Email: Ajs319@bath.ac.uk; K.A.Whitehead@mmu.ac.uk

Abstract

A commercial polylactic acid/graphene (8 wt.%) composite filament was used to additive manufacture (AM) graphene macroelectrodes (AM-G_{MS}). The electrode surfaces were characterised and *Pseudomonas aeruginosa* was selected as the exoelectrogen. The MFC was optimised using growth kinetic assays, biofilm formation, and quantification of pyocyanin production (*via* liquid chromatography-mass spectrometry) in conditions that were representative of the batch-fed MFC configuration utilised. Cell potential and bacterial viability was recorded at 0h, 24h, 48h, 72h, 96h and 120h, power density and current density were calculated. There was no significant difference between *P. aeruginosa* cell proliferation in either media tested, interestingly, no accumulation of pyocyanin was evident. Additively manufactured electrodes comprised of graphene (AM-G_{MS}) were successfully applied in a *P. aeruginosa* MFC configuration and power outputs ($110.74 \pm 14.63 \mu\text{Wm}^{-2}$) produced were comparable to that of the 'benchmark' electrode, carbon cloth ($93.49 \pm 5.17 \mu\text{Wm}^{-2}$). The AM-G_{MS} demonstrated power/current outputs similar to that of the carbon cloth electrodes in both anaerobic LB and glucose-based media over 120 h; the AM-G_{MS} had no significant detrimental effect on *P. aeruginosa* viability. This study highlights the potential application of additive manufactured electrodes with the incorporation of nanomaterials (*e.g.* graphene) as one approach to enhance power outputs.

Keywords: Microbial Fuel Cell; Additive Manufacturing; Graphene; *Pseudomonas aeruginosa*; Pyocyanin; Biotechnology.

Word Count: 7220

57 Abbreviations

Description	Identifier
Additive Manufactured Polylactic Acid	AM-PLA
Additive Manufacturing	AM
Additively Manufactured Graphene Electrodes	AM-G _{MS}
Average Roughness	S_a
Cationic Exchange Membrane	CEM
Closed Circuit Voltage	CCV
Colony Forming Units per mL	CFU mL ⁻¹
Crystal Violet Biofilm Assay	CVBA
E cell	Cell Potential
Fusion Deposition Modelling	FDM
Heterogeneous Rate Transfer Constants	k_{obs}^0
Liquid Chromatography Mass-Spectroscopy	LC-MS
Luria Bertani	LB
Microbial Fuel Cells	MFCs
Optical Density	OD
Polylactic Acid	PLA
Scanning Electron Microscopy	SEM

58

59

60

61

62

63

64

65

66

67

68

69

70

71

1.0. Introduction

Microbial fuel cells (MFCs) are systems in which microorganisms convert chemical energy to electrical energy, usually by utilising an organic electron donor [1]. Microbial fuel cells (MFCs) are an area of vast interest in biotechnology due to their remarkable versatility which includes ambient operating conditions, they can also be utilised as a dual-approach to both produce renewable energy production and treat wastewater [2, 3]. However, the application of MFCs at an industrially relevant scale is yet to be realised, due to issues with scalability, therefore it is imperative to enhance the overall system efficiency [4-6].

The manufacturing and assembly process of MFCs can be significantly improved *via* the generation of monolithic designs [7]. One possible route to achieve such designs and improve MFC architectures, electrodes and ion exchange membranes is additive manufacturing (AM), more commonly known as 3D-Printing. The application of additive manufacturing provides a unique platform for both the rapid design and fabrication of complex structures with novel materials [8-10]. Previously, such architectures were not feasible using more traditional manufacturing routes [11-13]. In an MFC, the anode must be conductive and also exhibit good biocompatibility to sustain bacterial growth, furthermore, a high degree of surface area has been shown to be advantageous [9]. In 2017, You *et al.* 3D-Printed the first polymer based electrode for MFC application, where the conductive polylactic acid (PLA) filament (ProtoPlant, USA) was printed as a rectangular mesh to provide greater surface area [7]. Whilst, the 3D-Printed electrodes obtained lower outputs than the conventional carbon veil electrodes tested, the results were promising [7]. In another study, porous carbon was fabricated *via* a controlled carbonation process. The 3D-Printed anodes (pore size: 300 μm) produced a maximum power density of $233.5 \pm 11.6 \text{ mW m}^{-2}$, which represented a significant improvement in electrochemical performance when compared to the 2D control (carbon cloth) which produced a maximum power density of $69.0 \pm 4.7 \text{ mW m}^{-2}$ [14]. The application of additive manufacturing clearly has unexploited potential which could enhance MFC power outputs.

Carbon-based materials are the most widely used electrode type in MFC configurations as microbial growth on the surface of metals can accelerate corrosion of the surface; metals submerged in aqueous solutions can produce metal ions [15-18]. Carbon cloth is one of the most widely utilised electrode materials and is often used as a benchmark in MFC studies [15, 19, 20]. Carbon cloth is an ideal electrode for MFC configurations as it demonstrates excellent electrical conductivity, good biocompatibility and a large surface area (due to enhance porosity). Carbon cloth is however excessively expensive for application in MFC

configurations (*ca.* USD\$ 1000 m⁻²) [21]. Therefore, a substantially cheaper (per 100 g) and more versatile electrode material was developed (Additive manufactured graphene macroelectrodes; AM-G_{MS}) and tested herein. Additive manufacturing equipment and raw materials (*i.e.* PLA) are relatively inexpensive and cost will continue to decrease as research and development into AM increases [22, 23]. Furthermore, Lanzotti *et al.*, (2019) demonstrated the use of recycled PLA as a viable option for AM, this would undoubtedly reduce material expenditure and provide a more economically sustainable, alternative electrode material for MFC configurations [24]. The incorporation of graphene into PLA filaments and other feedstocks for AM is one potential option for improving MFC electrode materials. Graphene, which is defined as a 2D monolayer lattice of sp² hybridised carbon atoms, has unique properties that make it an ideal electrode material. Such properties include: high electron conductivity, a large theoretical surface area and the ability to sustain high current densities [25-27]. The cost of the raw PLA/graphene composite filament is 100 USD /100 g, this is capable of producing *ca.* 13, 333 of the electrodes utilised throughout this study, offering a significant advantage over more expensive, traditional electrode material types [28].

Pseudomonas aeruginosa has previously demonstrated exoelectrogenic properties and thus this bacterium has been utilised in a number of MFC configurations [6, 29-31]. The power outputs obtained by *P. aeruginosa* MFCs can vary depending on a range of factors, which include, phenazine (*e.g.* pyocyanin) production, biofilm formation and flagella/pili (*i.e.*, nanowire) efficiency [31, 32]. The exoelectrogenic properties of *P. aeruginosa* is due to the production of soluble redox mediators, such as phenazines [33]. Phenazines exhibit electron transfer mediating properties by acting as electron shuttles, which can transfer liberated electrons to the anode of a MFC [34]. The most predominant and well-characterised natural phenazine secreted by *P. aeruginosa* is pyocyanin [29, 35]. The production rate of pyocyanin by *P. aeruginosa* is affected by a range of factors including, nutrient availability, physiological status and growth phase [29, 36]. The pyocyanin concentration of a MFC has a direct correlation with enhanced power generation, due to the ability of the phenazine to transport electrons through the bacterial cell membrane [30]. Interestingly, the addition of pyocyanin produced by *P. aeruginosa* can be utilised by other microorganisms (which may be incapable of pyocyanin production) in MFCs, thus resulting in enhanced current production [34, 37].

In this paper we report the fabrication and characterisation of the AM-G_{MS}, for the first time, produced from a commercially available polylactic acid (PLA)-graphene feedstock. These electrodes were then trialled, for the first time, in a MFC configuration and are shown to be comparable to (more expensive (when manufactured per meter)) carbon cloth electrodes.

2.0. Methods

2.1 Fabrication of additive manufactured graphene macroelectrodes (AM-G_{MS})

The AM designs utilised throughout this study were produced using a MakerBot Replicator + (Makerbot Industries, USA) fused deposition modelling (FDM) 3D-printer with a direct drive extruder at a temperature of 210 °C. A conductive polylactic acid (PLA) / graphene (8 wt%) composite filament (Black Magic 3D, USA) was 3D-printed into electrodes, known henceforth throughout this manuscript as additive manufactured graphene macroelectrodes (AM-G_{MS}). An unfilled (pure) PLA filament (AM-PLA), was used as the control throughout all of the experiments presented in this study. This AM-G_{MS} has a reported conductivity of 2.13 S/cm [13]. The AM-G_{MS} designs were drawn *via* Fusion 360 software (Autodesk, USA) to create a circular disc architecture with a diameter of 6.0 mm, thickness of 1.0 mm and theoretical surface area of 7.5 cm². A radial connecting strip (1.0 mm x 1.0 mm and 10.0 mm long) was also incorporated into the design to allow the simple connection of the electrode to the electrochemical system.

2.2 Bacterial Cell Culture

Prior to the start of the experiment, *P. aeruginosa* strain ATCC 9027 was cultured onto Luria Bertani (LB; BD Difco[™], UK) agar. Inoculated plates were incubated at 37 °C for 24 h in aerobic conditions. *Pseudomonas aeruginosa* strain ATCC 9027 was inoculated into 10 mL LB or glucose-based broth (10 g glucose, 5 g yeast extract, 6.8 g sodium bicarbonate and 8.5 g sodium phosphate monobasic per litre; [38]) and incubated in either aerobic or anaerobic conditions at 37 °C, with agitation for 18 h. For anaerobic conditions, cultures were purged with nitrogen for 30 min to generate an anaerobic environment using a silicon rubber septa (Suba Seal, Merck, UK). Cultures were vortexed (5 s) and centrifuged (2,342 g for 10 min). Bacterial pellets were re-suspended and cells were washed with 10 mL of sterile distilled water, followed by centrifugation (2,342 g for 10 min). The final pellet was resuspended in 10 mL of LB or glucose-based broth, whilst maintaining the required anaerobic conditions. Cultures were adjusted to an OD_{600 nm} of 1 (± 0.1) which equated to *ca.* 5.0 × 10⁸ CFU mL⁻¹.

2.3. Surface Topography

The AM-G_{MS} surface topography was measured using optical profilometry [39]. Briefly, the surface roughness was quantitatively defined through the measurement of average

roughness (S_a), using a Zometrics, Zegage 3D optical profiler (Zygo, USA) at $\times 50$ magnification. The image analysis software used was Zemaps (Version 1.14.38). To increase accuracy, only biological repeats where $> 90\%$ of the surface was characterised by the software were included in the surface analysis conducted ($n = 9$).

2.4. Scanning Electron Microscopy (SEM)

Scanning electron microscopy (SEM) was used to visualise the AM-G_{MS} and *P. aeruginosa* strain ATCC 9027 retention and subsequent biofilm formation. Following the termination of the MFC experimentation (after 120 h), the anode, cathode and cationic exchange membrane (CEM) were isolated and dried at room temperature in a Class 2 biosafety cabinet (Atlas Clean Air, UK). Samples were then prepared for SEM as described in [40] and [41]. Briefly, the samples were fixed in 4 % glutaraldehyde for 24 h at 4 °C. The samples were then rinsed with sterile deionised water and were subjected to an ethanol gradient (10 % to 30 %, 50 %, 70 %, 90 % and 100 % v/v ethanol), samples were dried by desiccation over 24 h and were sputter coated with gold (Polaron, UK) for 30 s (parameters: power 5 mA, 800 V, 30 s, vacuum 0.09 mbar, argon gas). Scanning electron microscopy (SEM) was then performed using a JEOL JSM-5600LV model SEM.

2.5. Biofilm Quantification

To quantify biofilm growth on the electrode surface in the MFC conditions utilised, a crystal violet biofilm assay (CVBA) was conducted. These conditions consisted of LB broth, incubated at 37 °C under static anaerobic conditions in an anaerobic cabinet (80% N₂ 10% H₂ 10% CO₂; Ruskin, Wales). Biofilm growth was determined at set time-points, namely 0 h, 1 h, 24 h, 48 h, 72 h, 96 h and 120 h. For *P. aeruginosa* biofilm formation, 1 mL of inoculated LB, with an OD_{600 nm} adjusted to 1.0 ± 0.1 was added to a 12-well, flat-bottomed culture plate, under anaerobic conditions ($n = 3$). The AM-G_{MS} were sterilised using 70 % ethanol (for 10 min) prior to experimentation and were added individually into the wells of a 12-well culture plate, with the inoculated broth, the lid was added and sealed using Parafilm® to prevent evaporation during incubation. The inoculated well plates were incubated at 37 °C under static anaerobic conditions for the aforementioned time-points.

Following the incubation period, the LB broth was removed and discarded, the electrodes were dried at room temperature for 1 h in a Class 2 biosafety cabinet (Atlas Clean Air, UK). The CVBA experiments were conducted as described previously [18].

2.6. Pyocyanin Quantification – Liquid Chromatography Mass-Spectroscopy (LC-MS)

Pseudomonas aeruginosa strain ATCC 9027 growth kinetic assays were conducted over 120 h in LB and glucose-based broth, in anaerobic and aerobic-to-anaerobic conditions. At each time point (0 h, 24 h, 48 h, 72 h, 96 h and 120 h), 6.1 mL aliquots were removed, 5 mL was used for pyocyanin quantification, 1 mL for optical density measurements and 100 µL for bacterial cell viability measurements. The 5 mL suspensions were centrifuged at 1,721 x g for 10 min. A volume of 1 mL of the supernatant was added to 300 µL of methanol (with 0.1 M formic acid). Samples underwent further centrifugation (10,625 x g for 20 min) and 400 µL of the supernatant was removed and added to 800 µL of sterile deionised water. Once the samples were vortexed, 1 mL of the solution was filter sterilised using 0.22 µm filters (Millex®, Ireland) and placed into 0.3 mL glass vials (Agilent, USA) for storage at -80 °C.

To quantify the production of the pyocyanin, standards of different pyocyanin concentrations were prepared from High Performance Liquid Chromatography (HPLC) grade pyocyanin (Merck, UK). One millilitre of methanol with 0.1 M formic acid was added to the ampule of pyocyanin. This was vortexed (5 s), giving an initial concentration of 5 parts per million (ppm). For the LC-MS experiments, 5 ppb and 50 ppb concentrations were prepared from the above stock solution. The 5 ppb and 50 ppb were analysed alongside the LC-MS experiments to provide a known standard baseline at two different concentrations, thus enabling comparison of pyocyanin production between microbial samples.

An Agilent LC-MS 6540 UHD Q-TOF (Agilent, USA) with an ACE UltraCore 2.5 µm SuperC18™ 100 mm x 2.1 mm column (Advanced Chromatography Technologies, Scotland) was used for LC-MS analysis. The polar solvent used was LC-MS grade H₂O with 0.1 % formic acid, whilst, acetonitrile with 0.1 % formic acid was the mobile phase solvent. The LC-MS analysis was conducted in positive ion mode at 45 °C with a MS range of 100 - 3,000, which was calibrated using four reference masses. A constant flow rate of 0.3 mL/min was maintained within the column for 30 min and 10 µL samples were taken from each pre-prepared sample vial.

The data generated from the LC-MS was multiple Agilent .D files. All the .D output files from the LC-MS were converted to an open source format (.mzXML) to facilitate further analysis, utilising the open source converter ProteoWizard MSConvert [42]. The peak-picking filter was chosen as this uses centroidisation, which facilitated the use of the feature detection algorithm, *centWave* to detect and compare close-by and partially overlapping features [43]. The .mzXML files were imported into MzMine2 for peak detection and analysis [44]. The m/z peak for pyocyanin was confirmed in both the 5 ppm and 50 ppm reference samples as 211.086,

which corresponded to the monoisotopic peak of pyocyanin (210.079) with the addition of $[M+H]^+$ peak [45]. This reference mass was selected as the targeted peak to be used with the peak detection function with the corresponding reported retention time. An intensity deviation tolerance of 50 %, noise level of 1.0×10^3 , m/z deviation of 5 ppm and retention time deviation of 10 % were selected. To quantify the amount of pyocyanin per sample, the response factor was used as described in [46], with the concentration for each sample determined by using the average calculated response factor for the two standards. The relative response factor was multiplied by 1000 to convert from mg mL⁻¹ to ppm. This value was divided by the calculated sample dilution factor for LC-MS preparation (which was 0.256) to determine the actual pyocyanin concentration at different time-points, per sample. Pyocyanin production per CFU mL⁻¹ was calculated, in order to determine if the growth media utilised resulted in a significant difference in pyocyanin production.

Datasets generated were analysed and the pyocyanin present quantified. Graphs were generated using the average sample concentration *via* GraphPad Prism (Version 8) and the standard error of the mean was notated using error bars.

2.7. Microbial Fuel Cell Configuration

2.7.1. MFC Construction

A classic H-shaped MFC device was utilised (Figure 1), which consisted of two microbial fuel cell glassware components (Adams & Chittenden Scientific Glass, USA), each with a total volume of 120 mL. The two compartments were separated by a cationic exchange membrane (CEM; CMI-7000, Membrane International, USA). Prior to use, all components were sterilised with 70 % ethanol. The anodic chamber consisted of 120 mL LB or glucose-based broth, which was degassed with nitrogen to remove dissolved oxygen to generate anaerobic conditions, prior to inoculation. An aliquot of 1 mL of prepared *P. aeruginosa* culture was added to the anodic compartment, resulting in a starting OD_{600 nm} of 0.01 (this equated to *ca.* 5.0×10^6 CFU mL⁻¹). The cathodic compartment consisted of 120 mL, 50 mM potassium hexacyanoferrate and 0.1 M potassium chloride (as the supporting electrolyte).

The AM-G_{MS}, AM-PLA and carbon cloth electrodes all have a geometric surface area of 7.5 cm² and were used (independently) for both the anode and cathode in each study. The electrodes were prepared by attaching the electrodes to 0.75 mm² stranded, tinned copper wire (Farnell, UK) *via* heat shrink tubing. The exposed surface between the electrodes and the heat shrink tubing was sealed with electrical tape and epoxy resin (Araldite®, Huntsman

Advanced Materials, Switzerland). This ensured the isolation of the wire to prevent direct electron transfer by *P. aeruginosa* and minimised the risk of antimicrobial copper ions being produced. Therefore, only the calculated surface area was available to partake in electron transfer. Each MFC configuration tested was carried out in biological triplicates ($n = 3$).

2.7.2 Measurement and Analysis

The MFC configuration was connected to a high-resolution ADC-24 (Pico technology, UK) data acquisition system via an Arduino UNO (Arduino, Italy), which was coupled to a 10 K Ω external resistor. The closed circuit voltage (CCV) reading was recorded every 24 h, which resulted in voltage readings at 0 h, 24 h, 48 h, 72 h, 96 h and 120 h, over the 120 h incubation period, using Picolog software (version 6.1.10). The CCV recorded at each time-point was used as the Ecell (cell potential (V)) and by using Ohm's law, power [47] and current [48, 49] densities were calculated:

Power density:

$$\text{Power Density (W m}^{-2}\text{)} = \frac{(\text{E Cell (V)})^2}{\text{Resistance } (\Omega) \times \text{Surface Area (m}^{-2}\text{)}} \quad [1]$$

Current density:

$$\text{Current Density (A m}^{-2}\text{)} = \frac{\text{E Cell (V)}}{\text{Resistance } (\Omega) \times \text{Surface Area (m}^{-2}\text{)}} \quad [2]$$

2.7.3 Bacterial Enumeration

Bacterial viability was determined at each time point (0 h, 24 h, 48 h, 72 h, 96 h and 120 h) by Miles and Misra assays [50]. Colonies were counted and viability (CFU mL⁻¹) was determined to generate growth curves that could then be compared against the power/current densities generated. Enumeration of bacterial cells was carried out in biological triplicates ($n = 3$).

2.8. Statistical Analysis

Statistical analysis was conducted by performing two-way ANOVA coupled with Tukey's multiple comparison tests for post hoc analysis using GraphPad Prism (version 8.4.2; GraphPad Software, USA) to determine significant differences at a confidence level of 95 %

($p < 0.05$). Error bars represent the standard error of the mean. Asterisks denote significance, $*(p \leq 0.05)$, $** (p \leq 0.01)$, $*** (p \leq 0.001)$ and $**** (p \leq 0.0001)$.

3.0. Results

3.1. Surface Topography Characterisation

The surface morphology of the AM-G_{MS} was examined using SEM (Figure 2.A.). At a relatively lower magnification (100×) the surface topography of AM-G_{MS} was revealed, a highly heterogenous topography was observed due to the striations created during the manufacturing process. In light of this, optical profilometry was used to further characterise the topographical features of both sides of the AM-G_{MS} (Figure 2.B.). Average surface roughness of the additive manufactured electrodes revealed a difference in surface topography when comparing the top and the underside of the AM-G_{MS} and the control, AM-PLA. The topside of the AM-G_{MS} surface produced an average roughness of 4.40 μm , compared to the underside of the same electrode (2.65 μm). This was due to the manufacturing process as the underside of the electrode was extruded on to the smooth flat bed of the 3D printer. Both sides of the AM-G_{MS} electrode exhibited a significantly greater surface roughness, than AM-PLA (containing no graphene). Only samples that had > 90 % of the surface analysed were included in this study to enhance accuracy and reliability.

3.2. Biofilm Quantification

In order to quantify biofilm growth, biofilm studies were run simultaneously with the MFC experimentation, which allowed biofilm growth on the electrodes to be studied without disturbing the potential difference produced in the MFC experiments (Figure 3). To assess biofilm formation *P. aeruginosa* strain ATCC 9027 was inoculated in anaerobic LB broth, as per the MFC experiment protocol. Both the AM-G_{MS} and AM-PLA electrodes were evaluated after the following time-points, 0 h, 1 h, 24 h, 48 h, 72 h, 96 h and 120 h. At each time-point, greater bacterial biomass was observed on the AM-G_{MS}, which was significant at 24 h ($p \leq 0.0001$), 48 h ($p \leq 0.0001$), 96 h ($p \leq 0.001$) and 120 h ($p \leq 0.01$) compared with the AM-PLA. A maximum biomass was recorded on the AM-G_{MS} at 48 h. However, after 48 h, a decrease in biomass was observed on both the AM-G_{MS} and AM-PLA electrodes respectively. The presence of graphene in the AM-G_{MS} enhanced *P. aeruginosa* biofilm formation when cultured in LB broth, under anaerobic conditions.

3.3. Pyocyanin Quantification – Liquid Chromatography-Mass Spectroscopy (LC-MS)

Pyocyanin production was quantified in parallel with the bacterial growth kinetics experiment, and samples were prepared after each time-point for LC-MS analysis (Figure 4). Overall, the results demonstrated little difference in the quantity of pyocyanin present when *P. aeruginosa* strain ATCC 9027 was grown in different growth media, namely, glucose-based and LB broth *P. aeruginosa* strain ATCC 9027 in anaerobic conditions (Figure 4.A.). The maximum amount of pyocyanin produced by *P. aeruginosa* strain ATCC 9027 in LB broth was 43.50 ppb after 24 h, and the maximum amount of pyocyanin produced by *P. aeruginosa* strain ATCC 9027 in glucose-based broth was 74.20 ppb after 0 h. However, no significant difference in pyocyanin production was observed when growth was conducted in glucose-based and LB broth.

Bacterial viability was calculated in colony forming units per mL (CFU mL⁻¹) (Figure 4.B.). To quantify the amount of *P. aeruginosa* strain ATCC 9027 present at set time-points bacteria were grown in the different growth media, namely, glucose-based and LB broth in anaerobic conditions. Anaerobic growth in both glucose-based broth and LB broth, resulted in traditional growth phase models, including the presence of lag phase, exponential growth (log phase), stationary phase and death phase. In the presence of LB medium, *P. aeruginosa* grew to a maximum of 2.94×10^7 CFU mL⁻¹, whilst, the highest recorded viability for an anaerobic *P. aeruginosa* culture in glucose-based medium was 1.3×10^7 CFU mL⁻¹.

The concentration of pyocyanin was then determined as a result of pyocyanin produced per CFU mL⁻¹ (Figure 4.C.). A significant increase in pyocyanin production was recorded in glucose-based broth at 2 h ($p \leq 0.01$) and 120 h ($p \leq 0.0001$) when compared to LB broth at the respective incubation time points.

3.4. Microbial Fuel Cell Analysis

Throughout MFC experimentation, the closed circuit voltage of the three electrode types (AM-G_{MS}, AM-PLA and carbon cloth) was recorded at 0 h, 24 h, 48 h, 72 h, 96 h and 120 h in two media types, anaerobic glucose-based and anaerobic LB (Figure 5.A.). The AM-PLA confirmed that the base material (with no graphene incorporated) demonstrated little conductivity. Both the AM-G_{MS} and carbon cloth electrodes demonstrated conductivity from 0 h to 24 h, which was monitored as an increase in cell potential. This was followed by a stationary period and finally from 72 h to 120 h a decrease in cell potential was observed. Interestingly, this correlated with the kinetics of bacterial viability, which were calculated at the same time-points (Figure 5.B.). The highest potential recorded was when *P. aeruginosa*

strain ATCC 9027 was inoculated with carbon cloth in anaerobic glucose-based medium after 96 h (324.00 ± 10.06 mV). The highest potential recorded from the AM-G_{MS} was in LB medium after 48 h (287.00 ± 18.52 mV). However, there was no statistical difference between the AM-G_{MS} in varying media.

During MFC experimentation, growth kinetic experiments were used to determine the viability of *P. aeruginosa* strain ATCC 9027 from MFCs over defined time-points (0 h, 24 h, 48 h, 72 h, 96 h and 120 h) (Figure 5.B.). All six conditions (three electrode materials \times two media sources) resulted in conventional bacterial growth phase models, including the presence of lag phase, exponential growth (log phase), stationary phase and death phase. The maximum viability was observed when *P. aeruginosa* strain ATCC 9027 was inoculated in anaerobic LB medium with carbon cloth electrodes after 72 h (6.94×10^7 CFU mL⁻¹). The maximum viability of *P. aeruginosa* strain ATCC 9027 in the presence of the AM-G_{MS} throughout this study was reported in anaerobic glucose-based broth after 96 h incubation (4.50×10^7 CFU mL⁻¹). There was no significant difference ($p > 0.05$) in cell viability when *P. aeruginosa* strain ATCC 9027 was grown in the presence of AM-G_{MS}, AM-PLA and carbon cloth electrodes in both glucose-based and LB broth, which indicated that the incorporation of graphene in the AM-G_{MS} resulted in no significant detrimental antimicrobial effect.

Power density was calculated from the cell potential values obtained during MFC experimentation using equation [1] (Figure 5.C). In the presence of *P. aeruginosa* strain ATCC 9027, the AM-PLA (no graphene) provided low power densities in both anaerobic glucose-based and LB broth (< 1 μ W m⁻²). The AM-G_{MS} and the carbon cloth electrodes recorded an increase in power density until 24 h, followed by a stationary period and then a decrease in power density from 96 h. The highest recorded power density from the electrodes used in this study was 110.74 ± 14.63 μ W m⁻², which was obtained from the AM-G_{MS} in LB medium after 48 h incubation. The highest recorded power density from the carbon cloth electrode was 93.49 ± 5.17 μ W m⁻² after 96 h incubation in anaerobic glucose-based broth. Statistical analysis revealed at 48 h that the AM-G_{MS} in LB broth (110.74 ± 14.63 μ W m⁻²) outperformed ($P \leq 0.05$) the carbon cloth electrode in anaerobic glucose-based broth (58.86 ± 10.84 μ W m⁻²). However, after 72 h ($p \leq 0.05$), 96 h ($p \leq 0.05$) and 120 h ($p \leq 0.01$) incubation, the carbon cloth electrode gave a greater current density than AM-G_{MS} in anaerobic glucose-based medium. This demonstrated that the carbon cloth electrodes in glucose-based broth were the most efficient electrode after 72 h incubation. There was no significant difference in power density between the AM-G_{MS} and carbon cloth electrodes when *P. aeruginosa* was incubated for 120 h in anaerobic LB broth.

Current density was also calculated from the MFCs, *via* the recorded potential values and equation [2] (Figure 5.D.). The highest current density achieved in this study was $382.67 \pm 24.69 \mu\text{A m}^{-2}$; this was calculated from the AM-G_{MS} in anaerobic LB broth after 48 h incubation with *P. aeruginosa* strain ATCC 9027. The highest current density achieved by the same electrode in anaerobic glucose-based broth was $284.00 \pm 10.36 \mu\text{A m}^{-2}$ after 24 h. The highest current density achieved by the carbon cloth electrode was $343.11 \pm 6.94 \mu\text{A m}^{-2}$ after 120 h incubation with *P. aeruginosa* stain ATCC 9027 in anaerobic LB medium. No significant statistical difference in current density was observed when *P. aeruginosa* was incubated over 120 h, in anaerobic LB broth and anaerobic glucose-based medium, in the presence of the AM-G_{MS} and carbon cloth electrodes. Therefore, both of these electrode materials showed comparable current and current density generation in a MFC configuration.

3.5. Bacterial Visualisation via SEM

Following 120 h incubation, the anode, cathode and the CEM surface, which was in contact the anolyte, were isolated and visualised *via* SEM (Figure 6). Visualisation of *P. aeruginosa* on the surface of the AM-G_{MS} in LB medium showed a sparsely populated surface (Figure 6.A.) when compared with the AM-PLA, which showed denser bacterial retention (Figure 6.D.). The cathode (AM-G_{MS}) in anaerobic LB broth showed no bacterial retention, indicating no bacterial transfer between the two chambers of the MFC (Figure 6.B.). The surface of the CEM isolated from the anodic chamber showed an abundance of *P. aeruginosa* retention, which was increased around surface defects (Figure 6.C.). The AM-G_{MS} in glucose-based medium (Figure 6.E.) demonstrated a thin and evenly distributed bacterial retention across the surface of the electrode. The AM-PLA electrode in glucose-based broth (Figure 6.F.) demonstrated enhanced bacterial retention around surface defects after 120 h of anaerobic incubation. This variation in bacterial retention may be due to the presence of graphene on the surface of the AM-G_{MS}.

4.0. Discussion

4.1. AM-G_{MS} Characterisation

4.1.1. Electrochemical Analysis of AM-G_{MS}

The AM-G_{MS} utilised throughout this study have previously been electrochemically characterised [13]. The heterogeneous rate transfer constants (k_{obs}^0), were found to correspond to $1.00 \times 10^{-3} \text{ cm s}^{-1}$ and $4.58 \times 10^{-4} \text{ cm s}^{-1}$ for the PLA / graphene filaments (prior to AM) and

the AM-G_{MS}, respectively, within a 1 mM hexaammineruthenium (III) chloride/0.1 M KCl solution [13]. The PLA / graphene composite filament exhibited faster electron kinetics than AM-G_{MS}, this could be due to improved percolation of agglomeration of graphene platelets in the filament prior to printing, once printed the dispersion of the graphene platelets improved, resulting in reduced percolation [13].

4.1.2. Surface Characterisation

A vital parameter to be considered when attempting to understand bacterial-surface retention is surface topography [51]. The size and shape of morphological features of a surface can directly influence bacterial retention [52]. Previous studies indicate that an increase in surface topography results in enhance bacterial retention and may also facilitate biofilm formation [53, 54]. Scanning electron microscopy of the topside of the AM-G_{MS} at $\times 100$ magnification revealed a striated surface morphology due to the FDM process; the circular cross-section of the extrudate from the print head, combined with relatively high melt viscosity and solidification on cooling, prevents melding into a microscopically flat surface. Instead a “log cabin texture” is produced, resulting in pits and grooves at a macro-scale level and enhanced bacterial retention, resulting in enhanced power outputs from the electrodes in an MFC configuration [55, 56]. The graphene aggregates in the PLA based composite led to local variations in solidification shrinkage and increased roughness of the AM-G_{MS} surface relative to the AM-PLA surfaces (which in comparison demonstrated a smoother surface topography). The micro-roughness on the striations in Figure 2 A is due to the graphene aggregates.

To further explore surface topography, both sides of the AM-G_{MS} and the AM-PLA electrodes were evaluated *via* optical profilometry and S_a (average surface roughness) values were recorded. Due to the fibrous nature of carbon cloth, surface characterisation by optical profilometry was not viable on this electrode material. The S_a values recorded revealed that that the topside of the AM-G_{MS} and AM-PLA electrodes resulted in a greater surface roughness when compared with the underside of the electrodes. The average surface roughness (S_a) of the AM-G_{MS} topside was 4.40 μm and for the underside it was 2.65 μm . The cell dimensions of *P. aeruginosa* are in the region of 0.5 μm - 1.0 μm (diameter) and 1.5 μm - 5.0 μm (length), therefore this difference in surface roughness could have a significant effect on bacterial retention [57, 58]. The optical profilometry results demonstrated that the additive manufacturing process did not yield homogeneous surfaces, the observed smoother underside of the electrodes was due to this surface being the first layer of the “print”, extruded onto the smooth flat bed of the 3D-printer [59], the extruded filament melt will mould to the smooth

bed surface before solidification, resulting in a smoother surface overall. The roughness values obtained in this study are in line with previously published literature [60].

The AM-G_{MS} electrodes have previously been characterised using Raman spectroscopy by [61]. The Raman spectra of the AM-G_{MS} feature the characteristic carbonaceous peaks, commonly referred to as the G and 2D (G') bands at *ca.* 1580 cm⁻¹ and 2690 cm⁻¹, respectively [62-64]. The graphene content of the AM-G_{MS} comprised of multi-layer graphene sheets, determined from the highly symmetrical 2D (G') band peak. Furthermore, there was a distinct lack of a characteristic shoulder on the 2D (G') band, which is commonly observed in graphitic materials [63, 65]. Whilst, the large D band was indicative of a high number of edge plane-like sites [66] which give rise to beneficial electron transfer sites, making it a useful electrode material.

4.2. Biofilm Quantification

Biofilm quantification was evaluated using predetermined MFC conditions (*P. aeruginosa* ATCC 9027 inoculated into LB broth at 37 °C under static, anaerobic conditions). *Pseudomonas aeruginosa* biofilm formation on the AM-G_{MS} was evaluated over 0 h – 120 h in anaerobic LB broth to replicate MFC conditions. Over the 120 h incubation period, greater biofilm formation was consistently evident on the AM-G_{MS} when compared to the AM-PLA counterparts. A peak in biomass was observed at 48 h and 72 h for the AM-G_{MS} and AM-PLA electrodes, respectively. The peaks were followed by a reduction in biomass, this could be due to biofilm detachment mechanisms which can be induced by environmental cues such as nutrient, pH and oxygen availability [67]. Therefore, the reduction in biofilm formation during the latter stages of the incubation period could be due to the anaerobic, nutrient-limited conditions that were utilised.

4.3. Pyocyanin Quantification – Liquid Chromatography-Mass Spectroscopy (LC-MS)

Pyocyanin production was quantified *via* LC-MS in parallel with each time-point of the growth dynamic experiment. The utilisation of different growth media can result in the production of different metabolites at varying concentrations [68], therefore LC-MS analysis was conducted on *P. aeruginosa* strain ATCC 9027 samples over 120 h in anaerobic LB broth and glucose-based broth. *P. aeruginosa* exhibited a significantly greater viability when inoculated in LB medium, compared to glucose-based broth under anaerobic conditions. Under anaerobic conditions, *P. aeruginosa* survival and proliferation is supported by mechanisms including denitrification, pyruvate fermentation and arginine fermentation [69, 70]. As *P.*

aeruginosa has no known nitrogen fixing ability, denitrification is not a viable survival pathway in this instance, however, it is potentially the fermentation of amino acids such as arginine that support proliferation in anaerobic LB medium [71]. To metabolise glucose under anaerobic conditions the Entner-Doudoroff pathway is used by *P. aeruginosa*, which converts one glucose molecule into two pyruvate molecules, resulting in the production of one ATP molecule and two excess reducing equivalents [72, 73]. The pyruvate can be further converted to acetate, producing additional ATP [73]. The results showed little variation in the concentration of pyocyanin produced by *P. aeruginosa* strain ATCC 9027 in the presence of anaerobic LB broth and glucose-based broth. The maximum concentration of pyocyanin in anaerobic glucose-based broth was 74.20 ppb at 0 h, whilst in anaerobic LB broth it was 43.50 ppb after 48 h incubation. Pyocyanin production was then quantified in regards to CFU mL⁻¹ obtained at each timepoint. A significant increase in pyocyanin production was recorded in glucose-based broth at 2 h and 120 h when compared to LB broth. This indicated that the glucose-based medium promoted the production of the electron shuttle, pyocyanin, when compared against LB broth, which could lead to further biological-based optimisation of MFC configurations in the future [6, 68, 74]. Throughout this study, pyocyanin accumulation was not evident over time. The fluctuations observed in the concentrations of pyocyanin may be a consequence of redox cycling, which can generate reactive oxygen species (ROS), such as H₂O₂, which can degrade pyocyanin [75, 76].

4.4. Microbial Fuel Cell Analysis

The AM-G_{MS} was applied in a MFC configuration, as PLA has excellent electrical insulation properties at < 70 °C [77, 78], another conductive control electrode, carbon cloth, was utilised for appropriate comparisons of the AM-G_{MS} to be made. Carbon cloth is widely applied as an electrode in MFC configurations due to its high conductivity, good biocompatibility and relatively large surface area [21]. However, it is excessively expensive as an electrode material in MFC configurations [21]. When inoculated with *P. aeruginosa* strain ATCC 9027, the AM-G_{MS} demonstrated excellent conductivity, producing a maximum potential (287 ± 18.52 mV). Carbon cloth produced a maximum potential in anaerobic-based glucose-based broth (324 ± 10.06 mV) whilst, the AM-PLA, which demonstrated limited conductivity, produced a maximum potential of (32 ± 1.01 mV).

In parallel to the cell potential recording every 24 h, a sample of the anolyte was taken (immediately after the cell potential recording, maintaining anaerobic conditions) and used to calculate cell viability. In all cases (three electrode materials in two types of media), *P.*

aeruginosa demonstrated typical growth kinetics. Interestingly, throughout this study there was no significant difference in cell viability between bacteria exposed to the AM-G_{MS}, AM-PLA and carbon cloth electrodes. This indicated that the presence of graphene within the AM-G_{MS} did not have a detrimental effect on *P. aeruginosa* viability. This appears to be contradictory to the reported controversial antimicrobial activity of graphene which is yet to be fully elucidated [79, 80]. Potential antimicrobial mechanisms of the graphene such as membrane perturbation, ROS generation and cellular wrapping are thought to be involved [79, 81, 82]. However, in this study, the AM-G_{MS} containing 8 wt.% graphene demonstrated no significant detrimental activity on *P. aeruginosa* viability.

Power and current densities were calculated using the recorded cell potential values from the MFCs. The highest current and power densities generated were $110.74 \pm 14.63 \mu\text{W m}^{-2}$ and $382.67 \pm 24.69 \mu\text{A m}^{-2}$, respectively. These values were calculated from *P. aeruginosa* strain ATCC 9027 in the presence of the AM-G_{MS} after 48 h anaerobic incubation in LB medium, under a fixed external resistor of 10 k Ω . The highest recorded power density was demonstrated by the carbon cloth electrode ($93.49 \pm 5.17 \mu\text{W m}^{-2}$ after 96 h) in anaerobic glucose-based broth. The highest recorded current density was $343.11 \pm 6.94 \mu\text{A m}^{-2}$ after 120 h incubation with *P. aeruginosa* stain ATCC 9027 in anaerobic LB medium. In a previous study that used a comparable MFC configuration, Jayapriya and Ramamurthy (2014), inoculated the anodic chamber with *P. aeruginosa* in a glucose-based medium (20 g peptone, 13.3 g glucose, 10 g potassium sulphate, 1.4 g magnesium chloride, per litre (pH 7.0)). Potassium ferricyanide was used as the catholyte and the resistor was fixed in the ohmic polarisation region. When carbon cloth was applied as both the anode and cathode in this configuration, a power density of $132.9 \mu\text{W m}^{-2}$ was recorded [83]. This indicates that the novel AM-G_{MS} utilised throughout this study demonstrated results that were comparable of that to the current benchmark electrode utilised in MFC configurations. As research in AM continues to expand, electrodes produced by this manufacturing technique will continue to become more efficient and less expensive [84]. One route to optimise the AM-G_{MS} to enhance power outputs in MFC configurations could be to increase the graphene concentration present. In a previous study Foster *et al.*, (2019) developed a bespoke PLA / graphene composite FDM filament with graphene content varying from 1 – 40 wt.% [85].

There was no significant difference in recorded power and current densities between the MFCs which utilised the AM-G_{MS}, compared with the more widely used carbon cloth electrode type, when used in the same medium over 120 h. The main restriction of MFCs for industrial applications is their low power densities (compared to other energy sources).

However, these results demonstrated that the novel utilisation of additive manufactured electrodes coupled with the addition of graphene can produce comparative outputs to the current ‘gold’ standard and with future research could enhance power outputs of MFC technologies [86].

4.5. Bacterial Visualisation via SEM

The anode, cathode and CEM were isolated after 120 h incubation and prepared for SEM in order to visualise *P. aeruginosa* retention to the MFC components. When the AM-G_{MS} were applied as the anode, in both anaerobic LB broth and glucose-based broth, the bacterial cell retention was sparse (when compared to the AM-PLA counterparts). This difference in cell retention may be due to the incorporated graphene, potentially due to modifications in surface energy and electrostatic interactions [87]. Biofilm composition, morphology, thickness and other physical properties play an integral role in bioelectricity production [88]. An increase in biofilm formation on the anodic surface has previously been shown to be directly proportional to MFC power outputs [89]. In light of this, in future studies the graphene content and surface properties could be modified (*via* AM parameters) and this could result in enhanced power and current densities.

5.0. Conclusions

Additive manufactured PLA/graphene (8 wt.%) composite electrodes (AM-G_{MS}) have been used in MFC applications for the first time. A commercial PLA/graphene (8 wt.%) composite FDM filament was used throughout the study. Raman Spectroscopy revealed that the AM-G_{MS} were comprised of multi-layered graphene. Optical profilometry revealed that the electrode surface in contact with the printer bed had a smoother topography than the top surface. The AM-G_{MS} had significantly higher surface roughness values when compared to the AM-PLA (control). Growth kinetics were measured to assess *Pseudomonas aeruginosa* viability in the presence of the electrodes and no significant detrimental activity was observed.

For the first time, AM-G_{MS} containing 8 wt.% graphene were utilised in a *P. aeruginosa* inoculated MFCs (using the conditions previously characterised), in two media types, anaerobic LB and anaerobic glucose-based broth. Over the 120 h incubation period the AM-G_{MS} exhibited good electrical conductivity and produced results comparable to that of a widely utilised ‘benchmark’ electrode material (carbon cloth). When inoculated in LB broth, in a *P. aeruginosa* MFC, the AM-G_{MS} produced power and current densities comparable to that of the current benchmark electrode of MFCs, carbon cloth, whilst being considerably less expensive and a more sustainable, environmental-friendly electrode material. Following MFC experimentation, SEM was conducted on the electrodes, whilst bacterial retention was sparse this did not affect the power outputs observed, and no detrimental antimicrobial effect due to the presence of graphene on the surface of the AM-G_{MS} was observed. In future research the surface profiles / morphologies of the AM-G_{MS} electrodes at the nano, micro and macro-scales could be optimised. Additionally, wastewater could be trialled as the anolyte AM-G_{MS} to further translate results to an industrial application. This study demonstrated the potential of additive manufacturing, coupled with the incorporation of nanomaterials for the fabrication of electrodes, to ultimately increase power outputs of MFCs.

5.1. Acknowledgements

The authors would wish to acknowledge technical support provided by Hayley Andrews (Manchester Metropolitan University).

5.2. Funding

The Manchester Fuel Cell Innovation Centre is funded by the European Regional Development Fund.

5.3. Author Contributions

K.A.W, C.E.B and A.J.S conceptualised the project. A.J.S., N.A.H., J.A.B. and C.M.L. were involved in data acquisition and analysis. D.W. designed and fabricated the voltammeter configuration used to monitor power outputs over time. K.A.W. and C.E.B. supervised the project and supplied the relevant materials. A.J.S drafted the final manuscript. All authors read and approved the final manuscript.

Figure 1. The two-chambered, classical H-shaped MFC utilised in this study. $\text{K}_3\text{Fe}(\text{CN})_6$, Potassium hexacyanoferrate (III), KCl; Potassium chloride, CEM; Cationic Exchange Membrane, Polytetrafluoroethylene; PTFE.

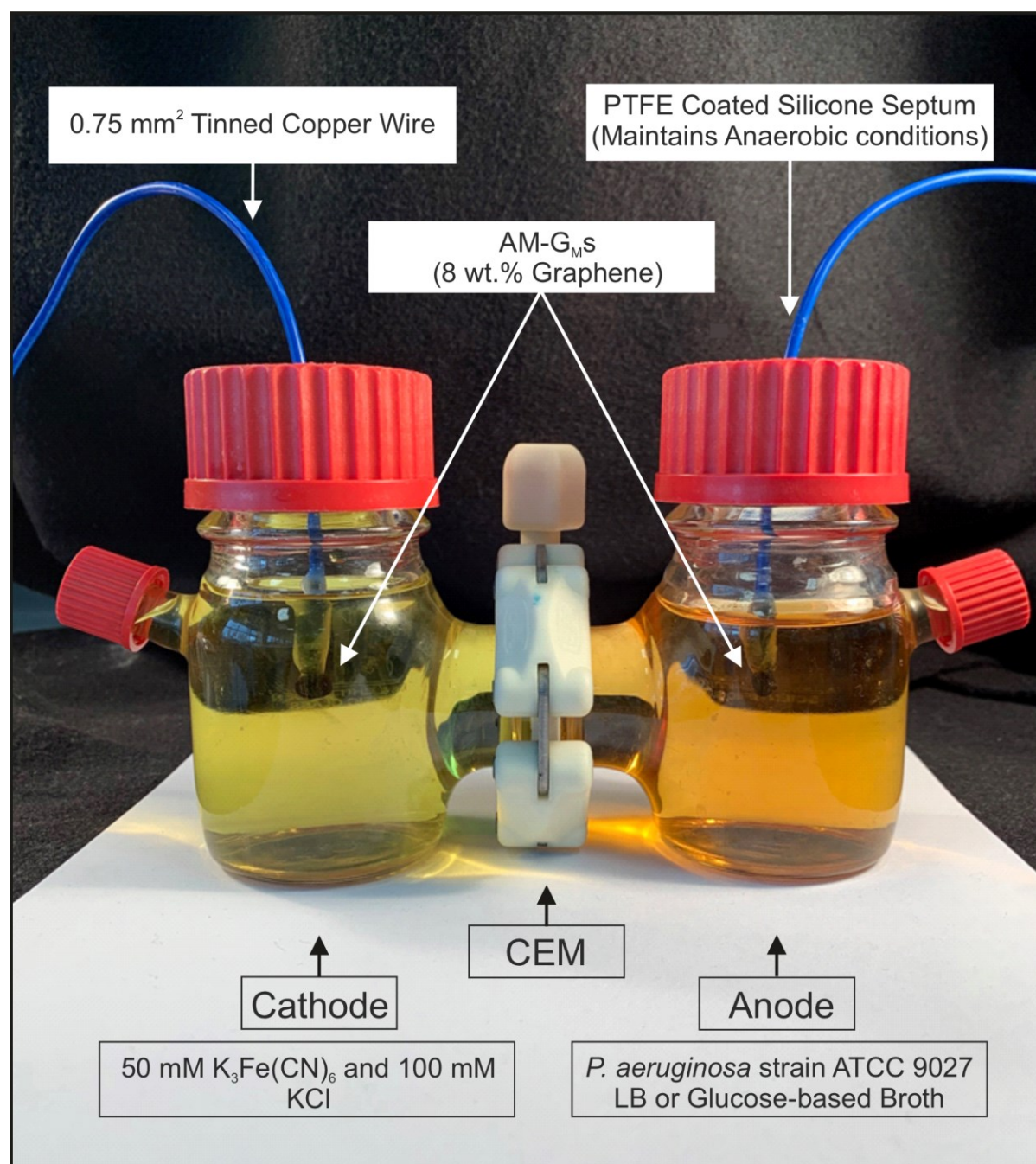


Figure 2. A. SEM image depicting the surface morphology of the AM-G_{MS} at 100 × magnification. **B.** Average surface roughness (S_a) of both sides of the AM-G_{MS} and the AM-PLA control ($n = 9$). Asterisks denote statistical significance, * ($p \leq 0.05$), ** ($p \leq 0.01$), and **** ($p \leq 0.0001$).

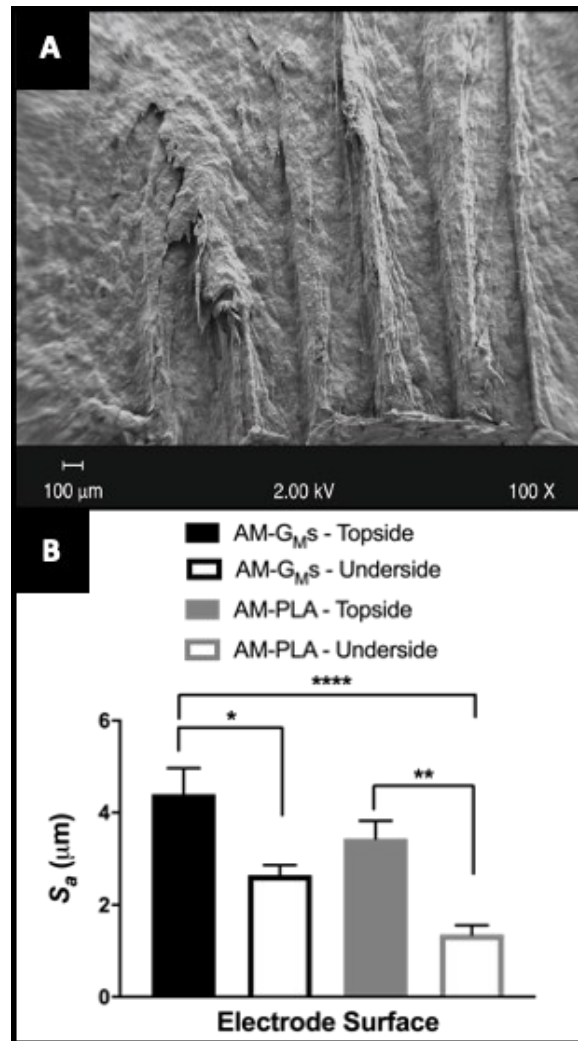


Figure 3. Biofilm quantification was determined using CVBA following *P. aeruginosa* strain ATCC 9027 incubation over 120 h in LB broth (deducting the sterile broth controls). Conditions replicated those selected for MFC experimentation (incubation conditions: static, LB broth, 37 °C, anaerobic) ($n = 3$). Asterisks denote significance, $** (p \leq 0.01)$, $*** (p \leq 0.001)$ and $**** p (\leq 0.0001)$.

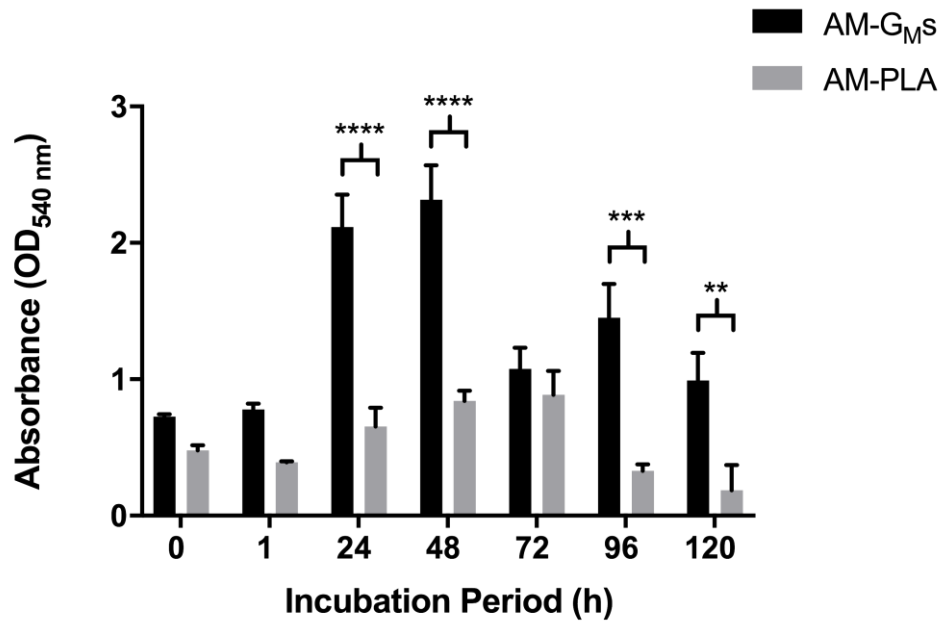


Figure 4. A. Growth kinetics were recorded by sampling *P. aeruginosa* strain ATCC 9027 over 120 h and conducting bacterial viability calculations, using two media types, glucose-based and LB broth (incubation conditions; anaerobic; 37 °C; static). **B.** Pyocyanin quantification *via* LC-MS from *P. aeruginosa* strain ATCC 9027 over 120 h **C.** Pyocyanin production normalised using growth kinetic data (CFU mL⁻¹) (*n* = 3). Where error bars are not visible they are of similar or smaller size compared to the symbol. Asterisks denote significance, *(*p* ≤ 0.05), **(*p* ≤ 0.01) and ****(*p* ≤ 0.0001).

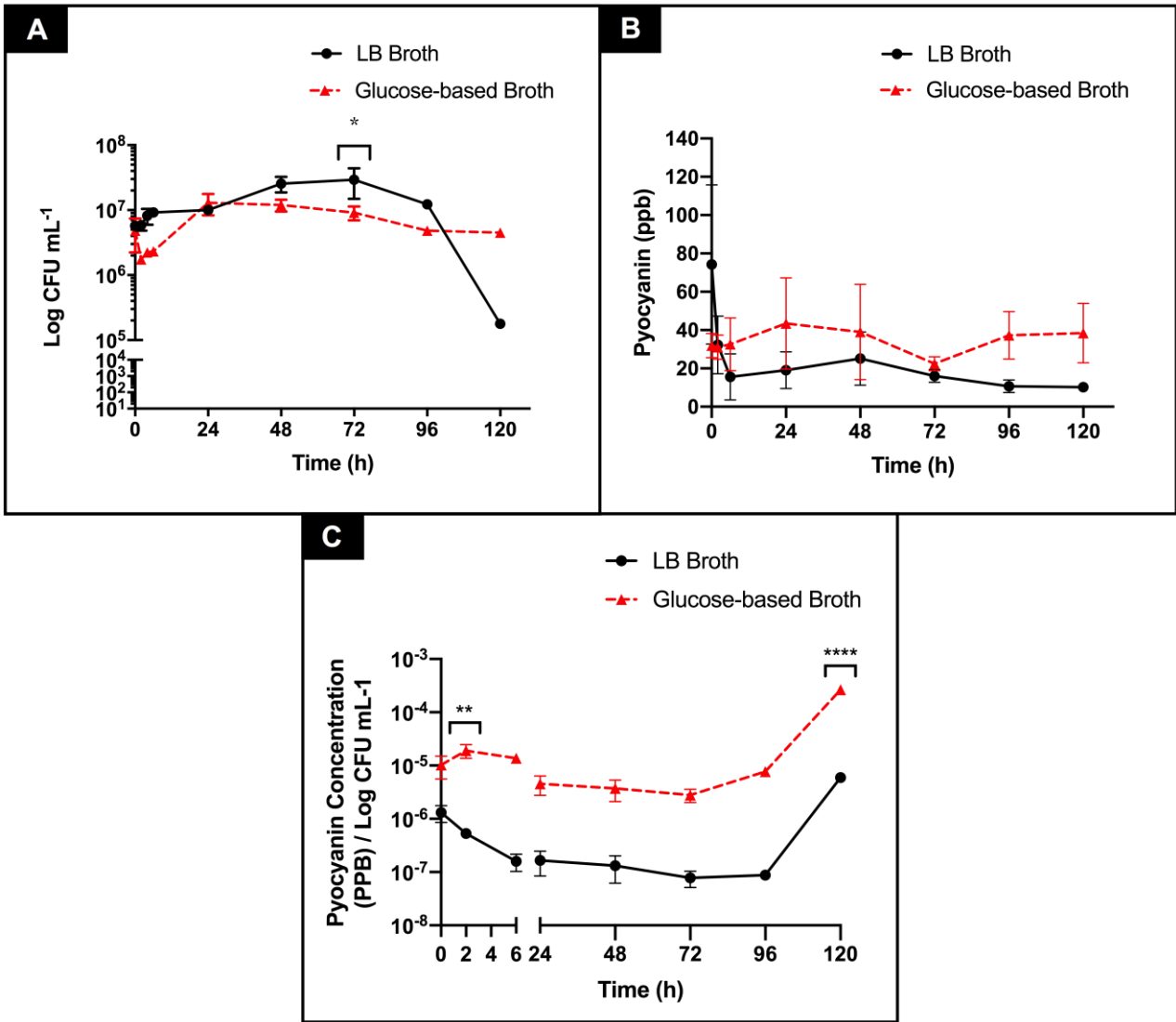


Figure 5. Microbial fuel cell configurations were trialled with the AM-G_{MS} inoculated with anaerobic *P. aeruginosa* strain ATCC 9027 MFCs ($n = 3$). **A.** Cell potential (V). **B.** Growth kinetics (CFU mL⁻¹). **C.** Power density ($\mu\text{W m}^{-2}$). **D.** Current density ($\mu\text{A m}^{-2}$). For the statistical analysis, only results between the AM-G_{MS} and carbon cloth electrodes were analysed, the black solid line denoted the different electrodes in glucose-based medium, the black dashed line denoted AM-G_{MS} in glucose-based broth against carbon cloth in LB broth, the red dashed line denoted the AM-G_{MS} in LB broth against carbon cloth in glucose-based medium. Asterisks denote significance, *($p \leq 0.05$), **($p \leq 0.01$), ***($p \leq 0.001$) and ****($p \leq 0.0001$).

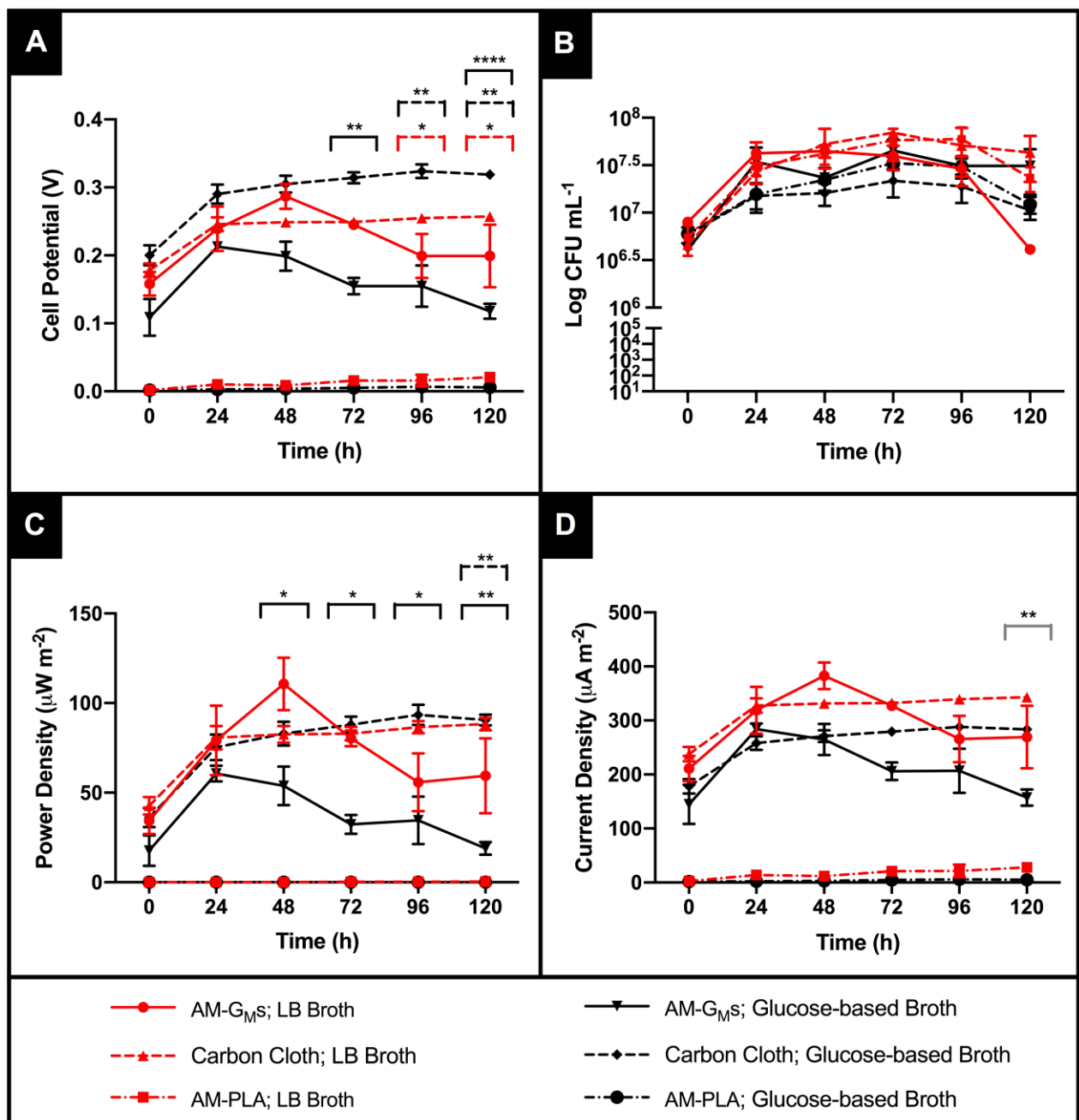
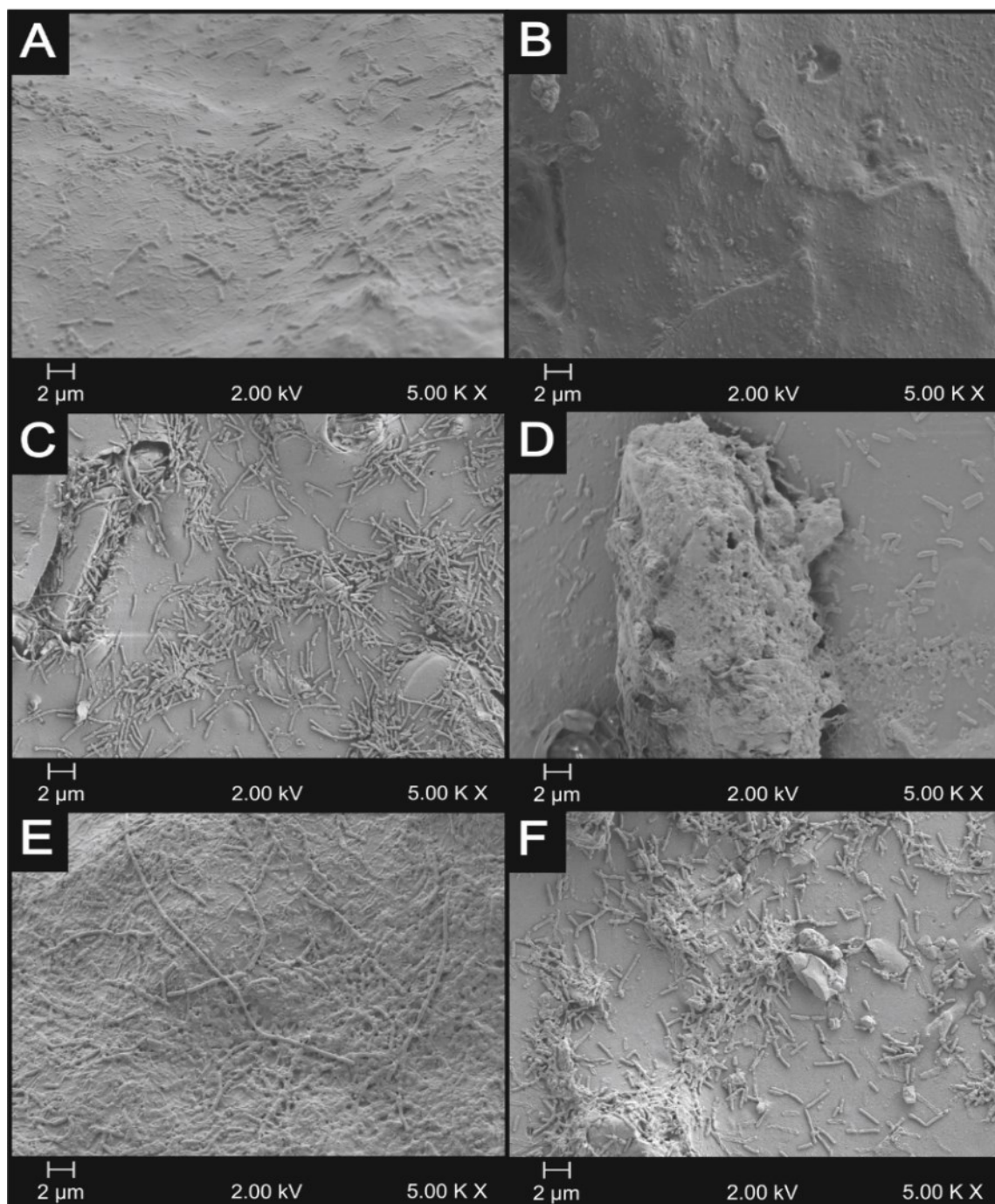


Figure 6. The electrodes and CEM were isolated post-MFC experimentation and *P. aeruginosa* strain ATCC 9027 was visualised using SEM (at 5.00 K \times magnification). **A.** AM-G_{MS} anode incubation in LB broth. **B.** AM-G_{MS} cathode (no bacteria present). **C.** CEM in LB broth (surface from the anodic compartment visualised). **D.** AM-PLA anode incubation in LB broth. **E.** AM-G_{MS} anode incubation in glucose-based medium. **F.** CEM in glucose-based broth (surface from the anodic compartment visualised).



6.0. References

- [1] V. Chaturvedi, P. Verma, *Bioresources and Bioprocessing*, 3 (2016) 38.
- [2] A. Rinaldi, B. Mecheri, V. Garavaglia, S. Licoccia, P. Di Nardo, E. Traversa, *Energy & Environmental Science*, 1 (2008) 417-429.
- [3] C. Santoro, C. Arbizzani, B. Erable, I. Ieropoulos, *Journal of Power Sources*, 356 (2017) 225-244.
- [4] B.E. Logan, *Applied Microbiology and Biotechnology*, 85 (2010) 1665-1671.
- [5] V. Oliveira, M. Simões, L. Melo, A. Pinto, *Biochemical Engineering Journal*, 73 (2013) 53-64.
- [6] A.J. Slate, K.A. Whitehead, D.A. Brownson, C.E. Banks, *Renewable and sustainable energy reviews*, 101 (2019) 60-81.
- [7] J. You, R.J. Preen, L. Bull, J. Greenman, I. Ieropoulos, *Sustainable Energy Technologies and Assessments*, 19 (2017) 94-101.
- [8] I.A. Ieropoulos, J. Winfield, J. Greenman, C. Melhuish, *ECS Transactions*, 28 (2010) 1.
- [9] F. Calignano, T. Tommasi, D. Manfredi, A. Chiolerio, *Scientific Reports*, 5 (2015) 1-10.
- [10] H. Philamore, J. Rossiter, P. Walters, J. Winfield, I. Ieropoulos, *Journal of Power Sources*, 289 (2015) 91-99.
- [11] R.D. Farahani, M. Dubé, D. Therriault, *Advanced Materials*, 28 (2016) 5794-5821.
- [12] E. MacDonald, R. Wicker, *Science*, 353 (2016) aaf2093.
- [13] C.W. Foster, M.P. Down, Y. Zhang, X. Ji, S.J. Rowley-Neale, G.C. Smith, P.J. Kelly, C.E. Banks, *Scientific Reports*, 7 (2017) 42233.
- [14] B. Bian, D. Shi, X. Cai, M. Hu, Q. Guo, C. Zhang, Q. Wang, A.X. Sun, J. Yang, *Nano Energy*, 44 (2018) 174-180.
- [15] M. Zhou, M. Chi, J. Luo, H. He, T. Jin, *Journal of Power Sources*, 196 (2011) 4427-4435.
- [16] F. Yu, C. Wang, J. Ma, *Materials*, 9 (2016) 807.
- [17] J. McBrearty, D. Barker, M. Damavandi, J. Wilson-Nieuwenhuis, L.I. Pilkington, N. Dempsey-Hibbert, A.J. Slate, K.A. Whitehead, *RSC advances*, 8 (2018) 23433-23441.
- [18] A.J. Slate, L. Shalamanova, I.D. Akhidime, K.A. Whitehead, *Letters in applied microbiology*, 69 (2019) 168-174.
- [19] M. Mashkour, M. Rahimnejad, *Biofuel Res. J*, 2 (2015) 296-300.
- [20] Y. Hindatu, M. Annuar, A. Gumel, *Renewable and Sustainable Energy Reviews*, 73 (2017) 236-248.
- [21] P. Choudhury, U.S. Prasad Uday, T.K. Bandyopadhyay, R.N. Ray, B. Bhunia, *Bioengineered*, 8 (2017) 471-487.
- [22] M. Altan, M. Eryildiz, B. Gumus, Y. Kahraman, *Materials Testing*, 60 (2018) 471-477.
- [23] A. Mitchell, U. Lafont, M. Hołyńska, C. Semprimoschnig, *Additive Manufacturing*, 24 (2018) 606-626.
- [24] A. Lanzotti, M. Martorelli, S. Maietta, S. Gerbino, F. Penta, A. Gloria, *Procedia CIRP*, 79 (2019) 143-146.
- [25] J. Moser, A. Barreiro, A. Bachtold, *Applied Physics Letters*, 91 (2007) 163513.
- [26] M.D. Stoller, S. Park, Y. Zhu, J. An, R.S. Ruoff, *Nano Letters*, 8 (2008) 3498-3502.
- [27] A.S. Mayorov, R.V. Gorbachev, S.V. Morozov, L. Britnell, R. Jalil, L.A. Ponomarenko, P. Blake, K.S. Novoselov, K. Watanabe, T. Taniguchi, *Nano Letters*, 11 (2011) 2396-2399.
- [28] G. Supermarket, in, *Graphene Laboratories Inc.*, 2020.
- [29] A. Price-Whelan, L.E. Dietrich, D.K. Newman, *Journal of bacteriology*, 189 (2007) 6372-6381.
- [30] H.-B. Shen, X.-Y. Yong, Y.-L. Chen, Z.-H. Liao, R.-W. Si, J. Zhou, S.-Y. Wang, Y.-C. Yong, P.-K. OuYang, T. Zheng, *Bioresource Technology*, 167 (2014) 490-494.

766 [31] N. Ali, M. Anam, S. Yousaf, S. Maleeha, Z. Bangash, Iranian Journal of Biotechnology,
767 15 (2017) 216.

768 [32] K. Rabaey, J. Rodríguez, L.L. Blackall, J. Keller, P. Gross, D. Batstone, W. Verstraete,
769 K.H. Neelson, The ISME Journal, 1 (2007) 9-18.

770 [33] E.M. Bosire, M.A. Rosenbaum, Frontiers in Microbiology, 8 (2017) 892.

771 [34] K. Rabaey, W. Verstraete, TRENDS in Biotechnology, 23 (2005) 291-298.

772 [35] L. Allen, D.H. Dockrell, T. Pattery, D.G. Lee, P. Cornelis, P.G. Hellewell, M.K. Whyte,
773 The Journal of Immunology, 174 (2005) 3643-3649.

774 [36] S. Romano, H.N. Schulz-Vogt, J.M. González, V. Bondarev, Applied and
775 Environmental Microbiology, 81 (2015) 3518-3528.

776 [37] M.E. Hernandez, A. Kappler, D.K. Newman, Applied and Environmental Microbiology,
777 70 (2004) 921-928.

778 [38] J. Liu, Y. Qiao, C.X. Guo, S. Lim, H. Song, C.M. Li, Bioresource Technology, 114
779 (2012) 275-280.

780 [39] A.J. Slate, D. Wickens, J. Wilson-Nieuwenhuis, N. Dempsey-Hibbert, G. West, P. Kelly,
781 J. Verran, C.E. Banks, K.A. Whitehead, Colloids and Surfaces B: Biointerfaces, 173 (2019)
782 303-311.

783 [40] M. Amin, S.J. Rowley-Neale, L. Shalamanova, S. Lynch, J. Wilson-Nieuwenhuis, M. El
784 Mohtadi, C.E. Banks, K.A. Whitehead, ACS applied materials & interfaces, (2020).

785 [41] J.A. Butler, A.J. Slate, D.B. Todd, D. Airton, M. Hardman, N.A. Hickey, K. Scott, P.D.
786 Venkatraman, Journal of Applied Microbiology, n/a.

787 [42] M.C. Chambers, B. Maclean, R. Burke, D. Amodei, D.L. Ruderman, S. Neumann, L.
788 Gatto, B. Fischer, B. Pratt, J. Egertson, Nature Biotechnology, 30 (2012) 918-920.

789 [43] R. Tautenhahn, C. Boettcher, S. Neumann, BMC Bioinformatics, 9 (2008) 504.

790 [44] T. Pluskal, S. Castillo, A. Villar-Briones, M. Orešič, BMC Bioinformatics, 11 (2010)
791 395.

792 [45] M. Kushwaha, S.K. Jain, N. Sharma, V. Abrol, S. Jaglan, R.A. Vishwakarma, ACS
793 Chemical Biology, 13 (2018) 657-665.

794 [46] M. Wang, C. Wang, X. Han, Mass Spectrometry Reviews, 36 (2017) 693-714.

795 [47] B.E. Logan, B. Hamelers, R. Rozendal, U. Schröder, J. Keller, S. Freguia, P. Aelterman,
796 W. Verstraete, K. Rabaey, Environmental Science and Technology, 40 (2006) 5181-5192.

797 [48] J. Teleken, J. Silva, M. Fraga, C. Oгородowski, F. Santana, B. Carciofi, Brazilian Journal
798 of Chemical Engineering, 34 (2017) 211-225.

799 [49] S.M. Imologie, O. Raji, A. Gbabo, C. Okoro-Shekwa, J. Renew. Energy. Environ, 3
800 (2016) 53-58.

801 [50] A.A. Miles, S. Misra, J. Irwin, Epidemiology and Infection, 38 (1938) 732-749.

802 [51] K.A. Whitehead, J. Colligon, J. Verran, Colloids and Surfaces B: Biointerfaces, 41
803 (2005) 129-138.

804 [52] L.C. Hsu, J. Fang, D.A. Borca-Tasciuc, R.W. Worobo, C.I. Moraru, Appl. Environ.
805 Microbiol., 79 (2013) 2703-2712.

806 [53] M. Katsikogianni, Y. Missirlis, Eur Cell Mater, 8 (2004) 37-57.

807 [54] W. Teughels, N. Van Assche, I. Sliepen, M. Quirynen, Clinical Oral Implants Research,
808 17 (2006) 68-81.

809 [55] L.C.d.M. Dantas, J.P.d. Silva-Neto, T.S. Dantas, L.Z. Naves, F.D. das Neves, A.S. da
810 Mota, International journal of dentistry, 2016 (2016).

811 [56] J. Liu, Y. Liu, C. Feng, Z. Wang, T. Jia, L. Gong, L. Xu, Energy Science & Engineering,
812 5 (2017) 217-225.

813 [57] E. Bédard, M. Prévost, E. Déziel, Microbiologyopen, 5 (2016) 937-956.

814 [58] I. Yoda, H. Koseki, M. Tomita, T. Shida, H. Horiuchi, H. Sakoda, M. Osaki, BMC
815 microbiology, 14 (2014) 234.

816 [59] T. Serra, J.A. Planell, M. Navarro, *Acta biomaterialia*, 9 (2013) 5521-5530.

817 [60] S.O. Akande, *International Journal of Engineering Research & Technology*, 4 (2015)

818 196-202.

819 [61] A.J. Slate, K.A. Whitehead, S. Lynch, C.W. Foster, C.E. Banks, *The Journal of Physical*

820 *Chemistry C*, 124 (2020) 15377-15385.

821 [62] D. Graf, F. Molitor, K. Ensslin, C. Stampfer, A. Jungen, C. Hierold, L. Wirtz, *Nano*

822 *Letters*, 7 (2007) 238-242.

823 [63] A.C. Ferrari, *Solid State Communications*, 143 (2007) 47-57.

824 [64] D. Yoon, H. Moon, Y.-W. Son, J.S. Choi, B.H. Park, Y.H. Cha, Y.D. Kim, H. Cheong,

825 *Physical Review B*, 80 (2009) 125422.

826 [65] S. Reich, C. Thomsen, *Philosophical Transactions of the Royal Society of London.*

827 *Series A: Mathematical, Physical and Engineering Sciences*, 362 (2004) 2271-2288.

828 [66] C. Casiraghi, A. Hartschuh, H. Qian, S. Piscanec, C. Georgi, A. Fasoli, K. Novoselov,

829 D. Basko, A. Ferrari, *Nano Letters*, 9 (2009) 1433-1441.

830 [67] K. Lee, S.S. Yoon, *Journal of Microbiology and Biotechnology*, 27 (2017) 1053-1064.

831 [68] N.A. Hickey, K.A. Whitehead, L. Shalamanova, J.A. Butler, R.L. Taylor, *Journal of*

832 *microbiological methods*, 163 (2019) 105647.

833 [69] K. Schreiber, N. Boes, M. Eschbach, L. Jaensch, J. Wehland, T. Bjarnsholt, M. Givskov,

834 M. Hentzer, M. Schobert, *Journal of Bacteriology*, 188 (2006) 659-668.

835 [70] C. Vander Wauven, A. Pierard, M. Kley-Raymann, D. Haas, *Journal of Bacteriology*,

836 160 (1984) 928-934.

837 [71] Y. Yan, J. Yang, Y. Dou, M. Chen, S. Ping, J. Peng, W. Lu, W. Zhang, Z. Yao, H. Li,

838 *Proceedings of the National Academy of Sciences*, 105 (2008) 7564-7569.

839 [72] T. Conway, *FEMS microbiology reviews*, 9 (1992) 1-27.

840 [73] N.R. Glasser, S.E. Kern, D.K. Newman, *Molecular Microbiology*, 92 (2014) 399-412.

841 [74] M.I. Rashid, S. Andleeb, in: *2018 International Conference on Power Generation*

842 *Systems and Renewable Energy Technologies (PGSRET)*, IEEE, 2018, pp. 1-6.

843 [75] A. Price-Whelan, L.E. Dietrich, D.K. Newman, *Nature chemical biology*, 2 (2006) 71-

844 78.

845 [76] K.J. Reszka, Y. O'Malley, M.L. McCormick, G.M. Denning, B.E. Britigan, *Free Radical*

846 *Biology and Medicine*, 36 (2004) 1448-1459.

847 [77] C. Dichtl, P. Sippel, S. Krohns, *Advances in Materials Science and Engineering*, 2017

848 (2017).

849 [78] T. Oi, K. Shinyama, S. Fujita, *IEEJ Transactions on Fundamentals and Materials*, 131

850 (2011) 395-400.

851 [79] H.M. Hegab, A. ElMekawy, L. Zou, D. Mulcahy, C.P. Saint, M. Ginic-Markovic,

852 *Carbon*, 105 (2016) 362-376.

853 [80] P. Kumar, P. Huo, R. Zhang, B. Liu, *Nanomaterials*, 9 (2019) 737.

854 [81] H.E. Karahan, C. Wiraja, C. Xu, J. Wei, Y. Wang, L. Wang, F. Liu, Y. Chen, *Advanced*

855 *healthcare materials*, 7 (2018) 1701406.

856 [82] A.J. Slate, N. Karaky, K.A. Whitehead, (2018).

857 [83] J. Jayapriya, V. Ramamurthy, *The Canadian Journal of Chemical Engineering*, 92 (2014)

858 610-614.

859 [84] C.Y. Foo, H.N. Lim, M.A. Mahdi, M.H. Wahid, N.M. Huang, *Scientific reports*, 8

860 (2018) 1-11.

861 [85] C.W. Foster, G.Q. Zou, Y. Jiang, M.P. Down, C.M. Liauw, A. Garcia-Miranda Ferrari,

862 X. Ji, G.C. Smith, P.J. Kelly, C.E. Banks, *Batteries & Supercaps*, 2 (2019) 448-453.

863 [86] D.Y. Lyon, F. Buret, T.M. Vogel, J.-M. Monier, *Bioelectrochemistry*, 78 (2010) 2-7.

864 [87] E. Zurob, G. Dennett, D. Gentil, F. Montero-Silva, U. Gerber, P. Naulín, A. Gómez, R.

865 Fuentes, S. Lascano, T.H. Rodrigues da Cunha, *Nanomaterials*, 9 (2019) 49.

866 [88] M.J. Angelaalincy, R. Navanietha Krishnaraj, G. Shakambari, B. Ashokkumar, S.
867 Kathiresan, P. Varalakshmi, *Frontiers in Energy Research*, 6 (2018) 63.
868 [89] C. Yuvraj, V. Aranganathan, *Arabian Journal for Science and Engineering*, 42 (2017)
869 2341-2347.
870